8

Small Ring Cyclodextrins : their Geometries and Hydrophobic Topographies

Abstract: A detailed force field-based evaluation of the molecular geometries of small ring cyclodextrins **1** – **3** (≡ *cyclo*[D-Glc*p*α(1→4)]*n*, *n* = 3 – 5) with three, four, and five α(1→4)-linked glucose residues, and the starch-derived α-cyclodextrin (**4**) was performed by using molecular mechanics and high temperature annealing. The resulting minimum energy structures reveal that the progressive strain imposed by diminution of the cyclodextrin macrocycle from six glucose units (α-CD, **4**) to five (cycloglucopentaoside **3**), four (tetraoside **2**), and three (cyclotrioside **1**), expresses itself in a widening of the intersaccharidic torsion angle, in a complex balancing of the interrelated glucose tilt angles τ and the glycosidic torsions Φ and Ψ against each other, and most strikingly, in a specific unilateral distortion of the pyranoid rings, i.e. flattening at C-4 towards the E_1 envelope conformation. This successive levelling at C-4, enabled by decrease of the two related ring torsion angles, is small in the pentamer **3**, pronounced in **2**, and fully realized in the cyclotrioside **1**. – The respective contact surfaces of the minimum energy conformers and their molecular lipophilicity patterns (MLP's), in color-coded form, were also generated, allowing an assessment of their capabilities to form inclusion complexes. Accordingly, only the cyclopentaoside **3** exhibits a hydrophobic center cavity similar to that of α-CD (**4**), the smaller cyclodextrins **2** and **1** are closed, yet contain a hydrophobic indentation for potential binding.

The native cyclodextrins **4** – **7** obtained from the action of *Bacillus macerans* amylase on starch, are cyclic oligosaccharides composed of six, seven, eight or nine α(1→4)-linked D-glucopyranose units[305-308]. All of these have been characterized by their X-ray structures[319,320] and a large body of information has accumulated on their ability to incorporate a variety of organic compounds into their cavity, both in the solid state and in solution[305-308].

Small-ring cyclodextrins:

1 *cyclo*[D-Glc*p* α(1→4)]$_3$
2 *cyclo*[D-Glc*p* α(1→4)]$_4$
3 *cyclo*[D-Glc*p* α(1→4)]$_5$

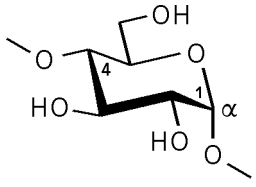

Starch derived cyclodextrins:

α-CD **4** *cyclo*[D-Glc*p* α(1→4)]$_6$
β-CD **5** *cyclo*[D-Glc*p* α(1→4)]$_7$
γ-CD **6** *cyclo*[D-Glc*p* α(1→4)]$_8$
δ-CD **7** *cyclo*[D-Glc*p* α(1→4)]$_9$

Although the cyclodextrin series may extend on the high molecular-weight side beyond the δ-cyclodextrin **7** at least up to the cycloglucododecaoside[440,441], no evidence has been brought forth that a cyclodextrin with less than six glucose

units – as, e.g. the cycloglucopentaoside **3** – is present in the amylose digestions of starch[440]. This abrupt termination of the series at the low molecular-weight side has, over the years, been commented in various ways. French, in 1957, remarked that the smallest cyclodextrin ring which can be constructed with space-filling models on the basis of $^4C_1$ conformations of the glucose units is the α-CD (**4**). However, when allowing boat or twist conformations for the pyranoid rings, "it is possible to construct essentially strainless cycloamylose rings having any number of D-glucose units from three to infinity"[440]. In 1970, on the basis of potential energy calculations it was inferred that "there is a drastic increase in energy when the number of D-glucose residues is less than six"[449], which was attributed to the fact that the diameter of a cyclodextrin with five or less sugar units cannot accommodate the 6-CH_2OH groups, which point approximately to the interior[449]. As recent as 1992, the non-existence of a cyclodextrin with fewer than six glucose units was rationalized to be due to "the high internal tensions which could then appear at the level of the ring"[316].

Whilst the glycosyltransferase from *Bacillus macerans* obviously is unable to generate cyclodextrins with fewer than six glucose units from starch, chemical synthesis is not, as convincingly evidenced by the recent straightforward preparation of the pentameric α(1→4)-linked cyclodextrin **3** via cyclization of a linear glucopentaose derivative[442]. In a similar fashion, the respective cyclomannin pentamer, i.e. the α(1→4)-linked all-*manno* analog of **3**, has been synthesized[443].

Accordingly, the early considerations of small-ring cyclodextrins[316,440,441,449] were obviously premature in their general as well as specific implications. Thus, it was necessary to subject the cyclodextrins **1** – **3** composed of three, four, and five glucose units, respectively, to a detailed molecular modeling study, knowledge of their geometries and molecular lipophilicity patterns (MLP's) conceivably allowing an assessment of their host-guest complexation capabilities.

Conformational Features of Small Ring Cyclodextrins in Relation to α-CD

The global conformation and the total molecular energy of the cyclodextrins depends on all of the intersaccharidic torsion angles Φ and Ψ, as well as the tilt angles τ of the individual glucose units that denote their inclination in relation to the macrocycle (cf. Fig. 6-1, right), while the pyranoses itself are comparatively rigid; all those molecular parameters are interrelated in a complex manner. For symmetrical structures, the internal degrees of freedom which have to be taken into consideration are considerably reduced, since then Φ and Ψ become an explicit function of τ. The torsion angles ω (Fig. 6-1, left) describe the orientation of the 6-OH groups with respect to the pyranoid ring, and thus, are related to local conformational aspects.

Geometry analysis of the small ring cyclodextrins **1 – 3** was performed by molecular mechanics using the PIMM91 force field program[45], thereby the native α-CD (**4**) – despite the availability of crystal structural data for different forms of its hydrate[337-339], and several molecular mechanics[331,332] and dynamics studies[333,334] – was included to unequivocally draw parallels to its small ring isomers independent of the mode of previous analyses. Of the various relevant variables that may be subjected to systematic permutation, the tilt angle τ, denoting the inclination of the pyranoid rings towards the mean plane of the cyclodextrin macrocycle (Fig. 6-1, right), and the torsion angle ω describing the conformation of the primary 6-OH in relation to the pyranoid ring (Fig. 6-1, left) were selected. After each step, the molecular geometries were fully energy-optimized.

The molecular parameters obtained in this way for the global minimum energy conformations of **1 – 4** are listed in Table 8-1, the resulting overall-geometries are depicted in Fig. 8-1, onto which, in addition, the MOLCAD-program[48] generated contact surfaces[46] were superimposed. As a consequence of the structure generation procedure, the PIMM91 minimum energy geometries exhibit symmetrical, almost perfectly planar *n*-polygons of all the O-1-atoms (root-mean-square displacements from planarity < 0.002 Å), and hence, can be regarded as the respective time-averaged "molecular images" of solution conformations.

In the case of α-cyclodextrin (**4**), the ball and stick model representation, and in more detail, the calculatory data in Table 8-1, reveal an essentially unstrained, torus-shaped macrocycle, with the primary 6-OH groups located on one side of the molecule, whilst the opposite aperture is made up by the secondary 2-OH and 3-OH groups. The intersaccharidic bond angle φ (C_1-O_1-$C_{4'}$), as well as the glycosidic torsion angles Φ and Ψ are within normal ranges. Good agreement is also observed for the alternate torsions Φ' (H_1-C_1-O_1-$C_{4'}$) and Ψ' (C_1-O_1-$C_{4'}$-$H_{4'}$) determined from ^{13}C-^{1}H-NMR-coupling constants of α-CD peracetate in $CDCl_3$ solution[324]. In particular, both the experimental and theoretical methodology estimate Ψ to be approximately 20 – 30° larger than Φ (Φ ≈ Φ' + 120° and Ψ ≈ Ψ' + 120°). The same holds for the tilt angle τ, its mean value of 109° clearly indicating the pyranoid rings to be inclined such that their 6-CH_2OH portions are turned towards the center cavity, forming the smaller opening, whilst the 2-OH / 3-OH section points away from the molecular axis, molding the wider torus rim.

However, measurement of ^{13}C-^{1}H-NMR-coupling constants yields the absolute values of |Φ'| and |Ψ'| only, yet, alignment of the monosaccharide units perpendicular to the macrocycle (τ ≈ 90°) corresponds to Φ' and Ψ'-torsions of approximately 0°, the

almost linear relationships of $\Phi' \approx 90° - \tau$ and $\Psi' \approx \tau - 90°$ would require the knowledge of at least one sign of Φ' and / or Ψ' for direct determination of τ.

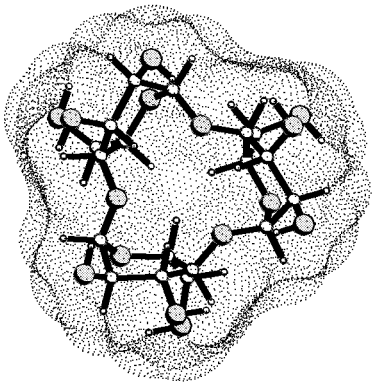

cyclo[D-Glc*p* α(1→4)]$_3$
1

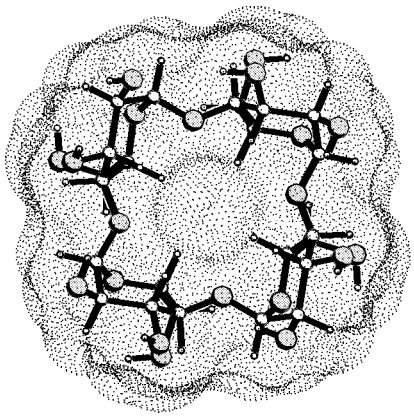

cyclo[D-Glc*p* α(1→4)]$_4$
2

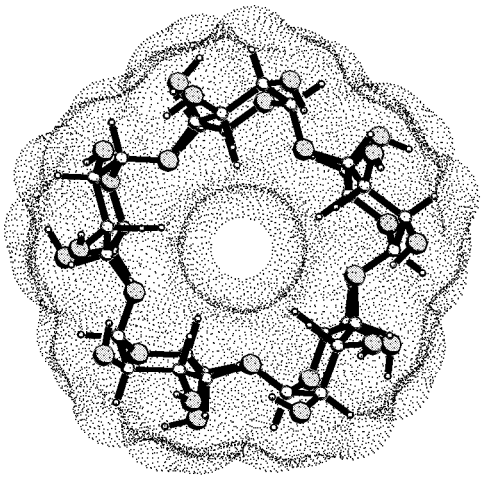

cyclo[D-Glc*p* α(1→4)]$_5$
3

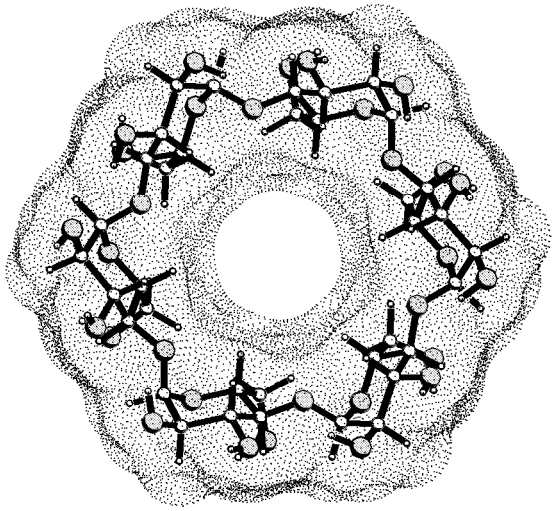

cyclo[D-Glc*p* α(1→4)]$_6$
4 (α-CD)

Fig. 8-1. Ball and stick model representations of the minimum energy structures (PIMM91) and dotted contact surfaces of the cyclodextrins **1** – **4** containing three, four, five, and six α(1→4)-linked glucose units, respectively. Structures are shown perpendicular to the mean ring plane of the macrocycles and are viewed through the large opening of the conically shaped molecules, i.e. the 2-OH / 3-OH side of the pyranoid rings points towards the viewer, and the primary 6-CH_2OH groups away from him, towards the back; oxygen atoms are shaded.

Table 8-1. Mean molecular geometry parameters of calculated cyclodextrin structures with three (**1**), four (**2**), five (**3**), and six (**4**, α-CD) glucose units in α(1→4)-linkages (root-mean-square deviations in parenthesis). For α-CD (**4**), the experimental data obtained from statistical analysis of crystal structures have been included for comparison.

cyclodextrin	intersaccharidic torsion angles[a] < Φ >	< Ψ >	bond angle[b] < φ >	tilt angle[c] < τ >	atomic distances [Å] < O_1-$O_{1n'}$ >[d]	< O_2-$O_{3'}$ >	< C_6-$C_{6'}$ >
Solid state structural data[e]:							
4 (α-CD)	107.4(6.6)	130.7(8.5)	118.2(2.0)	102.1(7.1)	8.51(0.23)	3.06(0.55)	4.45(0.21)
PIMM91 analysis[f]:							
4 (α-CD)	95.4(0.3)	138.7(1.1)	117.3(0.2)	109.0(0.2)	8.74(0.03)	3.30(0.04)	4.19(0.01)
3	102.4(0.7)	133.2(1.1)	117.8(0.2)	101.7(0.6)	6.53(0.02)	3.21(0.06)	4.51(0.01)
2	92.4(1.0)	141.0(0.7)	119.2(0.2)	104.6(0.7)	5.30(0.02)	3.75(0.07)	4.49(0.01)
1	81.7(0.1)	156.5(0.1)	123.5(0.1)	105.3(0.1)	3.32(0.01)	4.62(0.01)	4.74(0.01)
CHARMM HTA study[g]:							
4 (α-CD)	131. (11.)	111. (11.)	113.1(0.2)	85.7(10.)	8.21(0.08)	2.64(0.03)	5.23(0.35)
3	128. (10.)	113. (11.)	114.0(0.3)	88.7(8.6)	6.31(0.15)	2.73(0.35)	5.22(0.34)

cyclodextrin	pyranoid ring torsion angles[a] < $Θ_1$ >	< $Θ_2$ >	pyranose Cremer-Pople parameters < *Q* >	< θ >	< φ >	glucose conformation
Solid state structural data[e]:						
4 (α-CD)	52.3(5.1)	-53.0(6.2)	0.577(0.036)	5.7(4.8)	– [h]	$^4C_1$
PIMM91 analysis[f]:						
4 (α-CD)	46.9(0.7)	-47.0(0.2)	0.550(0.002)	9.0(0.3)	74.3(6.1)	$^4C_1$
3	39.4(0.9)	-39.6(0.1)	0.544(0.004)	18.0(0.2)	67.1(4.8)	$^4C_1$ (→ E_1)
2	30.5(0.3)	-28.6(0.4)	0.546(0.004)	28.9(0.3)	69.3(1.6)	E_1 (→ $^4C_1$)
1	11.8(0.1)	-6.1(0.1)	0.585(0.001)	48.8(0.1)	70.8(0.1)	E_1
CHARMM HTA study[g]:						
4 (α-CD)	45.5(1.7)	-49.9(1.4)	0.620(0.007)	14.8(1.4)	39.1(6.9)	$^4C_1$
3	39.0(2.3)	-43.5(2.6)	0.614(0.005)	20.9(2.1)	44.1(5.0)	$^4C_1$ (→ E_1)

a) Φ: O_5-C_1-O_1-$C_{4'}$, Ψ: C_1-O_1-$C_{4'}$-$C_{3'}$, $Θ_1$: C_2-C_3-C_4-C_5, $Θ_2$: C_3-C_4-C_5-O_5. – b) φ: C_1-O_1-$C_{4'}$. – c) angle between best-fit mean plane of the macro ring (defined by all O_{1n}-atoms) and each glucose-mean plane (atoms C_1 to C_5 and O_5). – d) O_1-O_{1n}-distances (in Å) diagonal across the cyclodextrin ring. – e) experimental values from 46 different solid state structures of α-CD and its inclusion complexes, including 54 crystallographically independent molecules. – f) calc. (PIMM91) for almost symmetrical, global minimum energy structures found. – g) calc. (CHARMM, High Temperature Annealing), Boltzmann-weighting of all HTA structures. – h) for $\theta \rightarrow 0°$, the puckering angle φ becomes meaningless, since $^4C_1$ conformations are identical to $^2C_5$ and $^0C_3$.

Table 8-2. Conformation of the glucose units in relation to the number of pyranoid rings in the macrocycle: going from the cycloglucohexaoside (**4**), via **3** and **2** to the cyclotrioside **1**, the ideal $^4C_1$ chair conformation is progressively bent towards E_1 envelope geometries by flattening at C-4 through decrease of the absolute values of the adjacent ring torsion angles $|\Theta_1|$ and $|\Theta_2|$. The steric strains and the geometrical requirements of the sugar units fitting into the small ring structures are displayed by the overall kink angle ε for each glucose residue.

cyclodextrin	mean geometry of pyranose units[a)]	kink angle[b)] < ε >	glucose conformation
cyclo[Glcα(1→4)]$_6$ (**4**, α-CD)	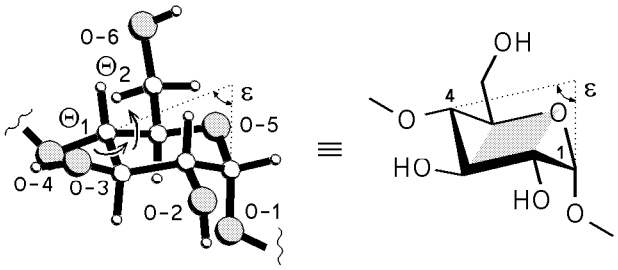	65.0±0.5°	$^4C_1$
cyclo[Glcα(1→4)]$_5$ (**3**)	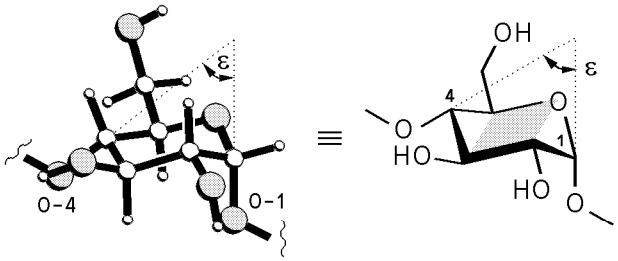	49.7±0.3°	$^4C_1$ (→ E_1)
cyclo[Glcα(1→4)]$_4$ (**2**)	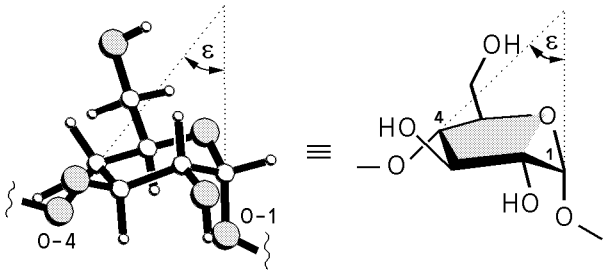	37.2±0.2°	E_1 (→ $^4C_1$)
cyclo[Glcα(1→4)]$_3$ (**1**)	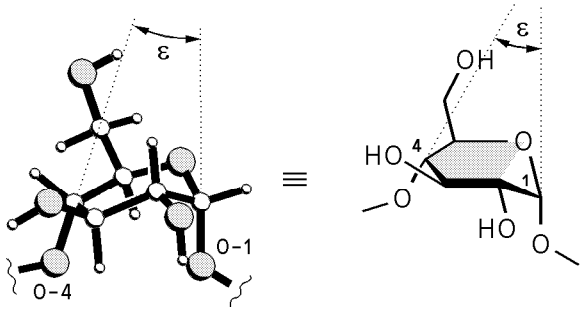	18.7±0.1°	E_1

a) global energy minimum structures (PIMM91), oxygen atoms are shaded, the relevant ring planes are indicated in the conformational pictograms. – b) angle between the C_1-O_1 and C_4-O_4 bond vectors for each glucose residue.

The pyranoid rings in α-CD (**4**) adopt a standard $^4C_1$ conformation as evidenced by the Cremer-Pople (CP) puckering parameters[122,124] and the torsion angles within the pyranose rings – only two, namely Θ_1 and Θ_2, describing the conformational relationships around C-4 are listed in Table 8-1 – that exhibit usual values ($\Theta_1 \approx +47°$ and $\Theta_2 \approx -47°$). These calculatory results are well corroborated by the data obtained from statistical analysis of altogether 46 different solid state structures of α-cyclodextrin and its inclusion complexes as retrieved from the Cambridge Crystallographic Data File[192,450] (cf. Table 8-1).

On proceeding from α-CD (**4**) to the smaller cyclodextrins **1** – **3** by successive excision of one glucose unit from the macrocycle, the variables that are balanced against each other are the intersaccharidic bond angle φ, the glycosidic torsion angles Φ and Ψ, the tilt of the pyranoid rings (τ), and the puckering of the glucose rings. The extent to which each of these parameters is affected in the calculatory energy minimum structures is revealed by the data in Table 8-1. The C_1-O_1-C_4 bond angle φ is successively widened, yet with minor effects in the cycloglucopentaoside (**3**) and the tetramer (**2**, $\Delta\varphi \approx +2°$), whilst the cycloglucotrioside **1** with $\varphi \approx 123.5°$ shows a 6° widening as compared to α-CD (**4**). Similar small reverberations are observed for the inclination of the pyranoid rings towards the center cavity, i.e. the tendency of the hydroxymethyl groups to be canted towards the center axis is uniformly maintained throughout the entire series. The tilt angles τ show only minor variation when proceeding from **4** → **1**, whilst the glycosidic torsion angles show opposite trends, Φ decreasing (≈ 100° → ≈ 80°) versus an increase of Ψ (≈ 135° → ≈ 155°). Thus, the geometrical constraints introduced into the macrocycle by reducing the ring size from six glucose units to five, four, and three, express themselves in a balancing of the three variables τ, Φ, and Ψ against each other. The values enforced in the cycloglucotrioside **1** are such, however, that an immense strain is to be surmised in the macrocycle, conceivably so high that the chances for this molecule ever to be synthesized are rather dim.

Another major effect in compensating the geometrical constraints imposed on the cyclooligoglucosides when proceeding from six to three glucose units, are the changes in pyranose conformations. The essentially normal $^4C_1$ chair of the glucose portions in α-CD (**4**) is only slightly distorted in the pentameric **3**: a slender flattening at C-4 towards the E_1 envelope, as indicated by the diminution of the two ring torsion angles (absolute values decrease by ≈ 7° each for Θ_1 and Θ_2), and the pyranose puckering parameters[451]. This trend continues more pronouncedly in the tetraoside **2** and reaches an essentially full E_1 envelope in the trioside **1** with Θ-values of +12° and -6° only. This is also manifested in the Cremer-Pople parameters: the puckering amplitude *Q*, i.e. the atomic mean-square deviation from planarity, is slightly higher in **1**

(≈ 0.59 Å) than in **2** – **4** (≈ 0.55 Å)*. Most notably, the parameter θ representing the latitude deviation of the spherical polar coordinate set [*Q*, θ, ϕ] changes from ≈ 5 – 10° in the case of α-CD (**4**) to ≈ 49° in the cycloglucotrioside **1**, while the nearly constant longitude of ϕ ≈ 65 – 75° indicates bending to occur particularly at C-4.

In a more transparent illustration, this trend from $^4C_1 \rightarrow E_1$ conformations may be described by the "overall kink angle" ε, defined as the angle between the C_1-O_1 and C_4-O_4 bond vectors of the respective glucose residues (cf. Table 8-2). The contraction of the macrocycle forces ε to become successively smaller, from 65° in α-CD (**4**) to 50° in the pentamer **3**, and to 37 and 19° in the cycloglucotetraoside **2** and trioside **1**, respectively.

In this context, it is to be noted that the increasing steric strain when going from the hexamer to the trimer expresses itself in flattening at the equatorial position of C-4 via decrease of the two related ring torsion angles Θ_1 and Θ_2, and not – at least not appreciably – at other positions of the pyranoid ring, e.g. at the anomeric carbon C-1. In considering this possibility, it becomes clear that bending of the pyranoid chair at C-1 would result in steric conflicts between the axial O-1, H-3, and H-5 atoms, and can only occur by an increase of two corresponding ring torsion angles (C_2-C_1-O_5-C_5 and C_3-C_2-C_1-O_5, respectively). Obviously, compensation of steric strain in pyranoid rings is energetically considerably more favorable through diminution of torsion angles than by their enlargement. This supposition receives support from the cyclogalactins evaluated in a modeling study (this work, Chapter 9): in the all-*galacto* analogs of **3** and **4** – both glycosidic linkage positions within the pyranoid rings are inverted (→ β(1→4)-*galacto*, hence: "*inverso*-cyclodextrins") – flattening occurs at the opposite side of the pyranose rings at C-1 (in this case, the CP-parameter ϕ becomes ≈ 230°) when proceeding from the cyclogalactohexaoside to the respective pentamer, since here the two ring torsion angles involved can effect this by diminution of their values, rather than by their energetically less favored enlargement.

Most impressively, the origins of strain inherent in the cycloglucotrioside **1** are visualized by MOLCAD-program[48] mediated color-coded projection of fragmental energetic contributions to the total strain energy (PIMM91[45]) onto ball and stick models[453] (Fig. 8-2), wherein red colors indicate high-energy bending. In **1**, the glycosidic angle at O-1 (φ ≈ 123.5°) is the most strained bond angle (Fig. 8-2, left), an

* For six-membered rings three polar-coordinate type Cremer-Pople (CP) parameters[122,124] *Q*, θ, and ϕ are necessary to describe the ring conformation. The puckering amplitude *Q* serves as a measure of the ring distortion only, being related to a mean-square atomic deviation from planarity. The angles θ (latitude) and ϕ (longitude) describe the ring conformation, e.g. θ ≈ 54.7° / ϕ ≈ 60.0° corresponds to an E_1-geometry, while θ ≈ 0.0° (in polar coordinates ϕ becomes meaningless for θ → 0°) is found for $^4C_1$-geometries.

effect that is propagated to a minor extent towards C-2 and C-3 of the glucose units. The torsional strain energy centered around C-4 and C-5 (Fig. 8-2, middle) originates from large distortions of the pyranoid units towards the less stable E_1 conformation and bending of Θ_1 and Θ_2 (*vide supra*). Torsion bending also affects the whole backbone of the macrocycle, including the intersaccharidic linkage (Φ and Ψ). The computed distortions originate mainly from close van der Waals contacts (Fig. 8-2, right) between the axial H-5 atoms pointing towards the molecular center (H-5 / H-5'-distances of approx. 1.91 Å only), which are minimized by energetically less costly bending of bond angles and torsions.

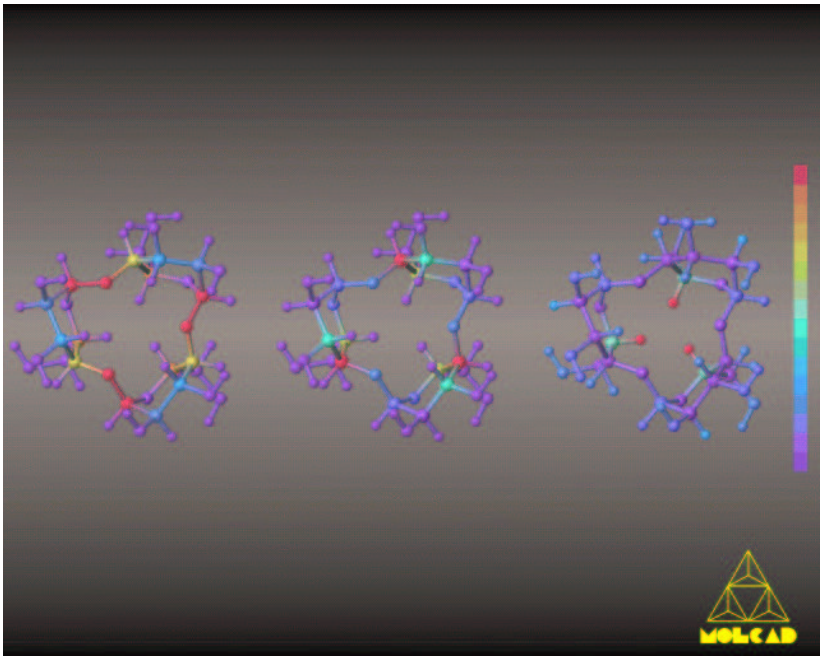

Fig. 8-2. Cyclo-α(1→4)-glucotrioside **1**: MOLCAD-program generated representation of the fragmental energetic contributions of angle bending (*left*), dihedral distortions (*center*), and van der Waals interactions (*right*) to the total PIMM91-strain energy. For visualization, a 16 color-code was used and projected on a ball and stick model each, red colors corresponding to high internal strain energies, violet colors indicating unstrained molecular fragments.

The rotamer population of the hydroxymethyl groups in relation to the pyranoid rings[66] is generally characterized in such, that of the three staggered conformations the *trans-gauche* (*tg*) form is the least favored due to 1,3-diaxial-like repulsions between O-4 and O-6[53,67-73]. None of the PIMM91 generated minimum energy structures (Fig. 8-1) contains such an unfavorable *tg* arrangement. Instead, for α-CD (**4**) and its small ring analogs **1** – **3**, the *gauche-gauche* (*gg*) rotamers emerge as the most stable ones, whilst – most pronouncedly in the cyclodextrins **1** and **2** – the *gauche-trans* (*gt*) forms have considerably higher energies, respectively. In the *gt*

form, the 6-CH_2OH-groups point towards the center axis of the cyclodextrins, whilst the *gg* rotamers – directed towards the outside – are generally favored unless intermolecular hydrogen bonding with guest molecules included in the center cavity can take place[327].

The atomic distances between O-2 of one glucose and O-3 of the next listed in Table 8-1, reflect the geometrical constraints and pyranoid ring distortion on diminishing the number of glucose units in the cyclodextrins **4** → **1**. These separations become significantly larger in **2** and **1**. In α-CD (**4**), the distances of ≈ 3.1 – 3.3 Å between adjacent 2-OH and 3-OH groups allow for strong intramolecular hydrogen bonding interactions, as was confirmed experimentally in solid state structures[327,328] as well as in solution[329]. These hydrogen bonding interactions not only explain the chemical inertness of the 3-OH groups[329], but as well the high 2-*O*-selectivity of base-induced alkylations of α-CD (**4**)[330], since the intermediate alkoxide anions are most efficiently stabilized via interresidue H-bonding at the 2-*O*-position[139]. On the basis of the data computed for the pentamer **3** (≈ 3.2 Å) it should be amenable to similar hydrogen bonding between the 2-OH and 3-OH groups. However, in the cyclotetraoside **2** and the trioside **1** the O_2-$O_{3'}$-distances are too large to be compatible with interresidue hydrogen bonding.

High Temperature Annealing of α-CD and Cycloglucopentaoside

Inasmuch as symmetrical structures have been criticized not to represent the global minimum energy conformations of cyclodextrins[331,332], the validity of the PIMM91[45]-results discussed above were checked through application of another force field (a modified CHARMM force field adapted to carbohydrates[454] and successfully tested for glycol and cellulose[455]). In addition, another computational methodology for exploring the accessible conformational space more exhaustively was used, i.e. High Temperature Annealing (HTA)[456], which ensures that – at least after long enough simulation times – all low-energy geometries are being seized.

During HTA simulations[456], molecular structures are drawn in regular time steps from a high temperature (1200 K) molecular dynamics (MD) trajectory and are slowly cooled down to 300 K in order to avoid ending up in irrelevant high energy minima, subsequently all structures obtained are fully energy minimized using molecular mechanics (MM). The MD simulation allows for Boltzmann weighted averaging of all molecular parameters over the entire set of geometries in consideration of the total cyclodextrin energy, computed values are included in Table 8-1, and the global minimum energy structures are shown in Fig. 8-3.

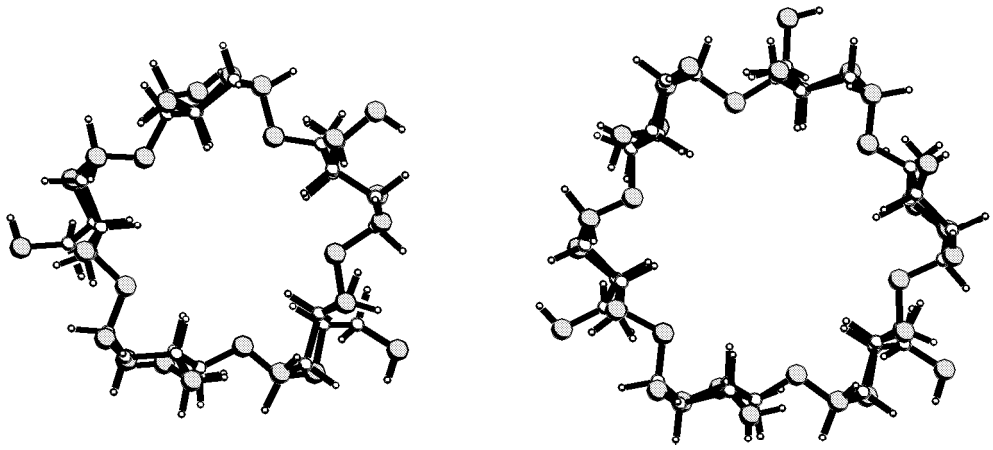

cyclo[D-Glc*p* α(1→4)]$_5$
3

cyclo[D-Glc*p* α(1→4)]$_6$
4 (α-CD)

Fig. 8-3. Molecular geometries of the HTA-derived global minimum energy structures (modified CHARMM force field) of cycloglucopentaoside (**3**, *left* side) and α-CD (**4**, *right* side). The mode of viewing was chosen cf. Fig. 8-1.

For both cyclodextrins **3** and **4**, respectively, the structural descriptors differ significantly from those obtained from the PIMM91 analysis. Most notably, the tilt angles ($\tau \approx 85 - 90°$, cf. Table 8-1) indicate the glucose units to line up almost perpendicular in respect to the macrocycle, with the 6-OH groups being turned slightly towards the outside. As compared with the PIMM91 geometries, the changes in τ ($\Delta\tau \approx 10 - 20°$) account for the increase of Φ ($\rightarrow \approx 130°$) and decrease of Ψ ($\rightarrow \approx 110°$), as well as for a widening of the torus rim at the 6-OH side (increased C_6-$C_{6'}$-distances of ≈ 5.2 Å) and a simultaneous contraction of the opposite aperture made up by the 2-OH and 3-OH groups (decreased O_2-$O_{3'}$-distances of ≈ 2.7 Å). Obviously, all these effects originate from an overestimation of hydrogen bonding energies between the 2-OH and 3-OH groups of adjacent glucosyl units[457]. In consequence, the HTA-structures exhibit a less conical, but more cylindrical overall shape than the PIMM91 geometries. The *n*-polygon of all the O_1-atoms forms almost planar structures in **3** and **4** (calc. root-mean-square atomic displacements from planarity ≈ 0.05(4) Å and ≈ 0.10(9) Å, respectively) and no significant puckerings for the entire macrocycles are computed.

These results are in contrast to a previous MM2 and AMBER MM-analysis[332], which indicates significant large distortions of the whole cyclodextrin ring. In this study[332], the torsion angles $\theta_{O\text{-}O}$ formed by four consecutive glucose-linking O-1-atoms found for the α-CD structures are obviously overestimated ($|\theta_{O\text{-}O}|$ up to

33°), when comparing the data with the rather small values observed in α-CD crystal structures[192,450] (mean value $<|\theta_{O\text{-}O}|> \approx 5.1 \pm 3.3°$, $|\theta_{max}| = 16.8°$). Symmetry breaking of cyclodextrins was found to lower their potential energy substantially, and thus, symmetric structures of cyclodextrins may be considered as time-averaged views only[332]. Indeed, the CHARMM global minimum energy structure of α-CD (**4**) exhibits 3-fold rotational symmetry, and many of the energetically favorable structures are characterized by C_2- or C_3-symmetry, no C_6- or C_5-symmetrical geometries were found for α-cyclodextrin (**4**) or its pentameric analog **3**, respectively. However, the differences of the tilt angles between joined glucose units are rather small: for α-CD (**4**) the average mean difference $<|\Delta\tau|> = 16.0 \pm 8.3°$ was calculated ($<|\Delta\tau|> \approx 6.4°$ for the global minimum structure), in **3**, $<|\Delta\tau|>$ amounts to $6.9 \pm 8.1°$ only ($<|\Delta\tau|> \approx 4.7°$ for the global minimum).

Going from α-CD (**4**) to the pentamer **3**, slight flattening of the pyranose $^4C_1$ conformations at C-4 is indicated by decrease of the ring torsion angles Θ_1 and Θ_2 by approx. 6° each, and in particular, by increase of the Cremer-Pople puckering parameter θ ($\approx 15° \rightarrow \approx 21°$, with $\phi \approx 40 - 45°$, cf. Table 8-1). The puckering amplitude Q of approximately 0.61 – 0.62 Å may be slightly overestimated by the CHARMM force field. It is noteworthy that the calculated changes in Θ_1, Θ_2, and θ upon excision of one glucose unit from the macrocycle (**4** → **3**) are larger than the corresponding root-mean-square fluctuations, and thus are obviously significant.

On the basis of multiple conformational transitions observed for the glucose units during the HTA simulation, the fully relaxed energy potential surfaces as a function of the pyranose puckering parameters Q, θ, and φ were calculated for the cyclodextrins **3** and **4** (α-CD). The resulting three-dimensional iso-energy contour maps are plotted in polar coordinates (Fig. 8-4, left), and their projections into the equator plane are depicted alongside (Fig. 8-4, right), allowing to correlate the total molecular energy of each cyclodextrin with distinct conformations of the glucopyranose units, respectively.

For α-cyclodextrin (**4**), a narrow and steep-contoured energy minimum close to the northern apex ($\theta \approx 10 - 15°$) of the Q / θ / φ-hypersurface of conformational states reveals almost unstrained $^4C_1$ geometries as the most stable conformations for the glucopyranose units. A shallow minimum barely below the +50 kJ/mol level in the $^1S_3$-skew (twist boat) region – i.e. distortion of at least one glucose residue towards a $^1S_3$ conformation increases the total molecular energy of **4** by approximately 50 kJ/mol – indicates that distorted pyranose conformations will be adopted only if α-cyclodextrin is perturbed by strong forces such as, for example, strong interactions with encapsulated guest molecules[321].

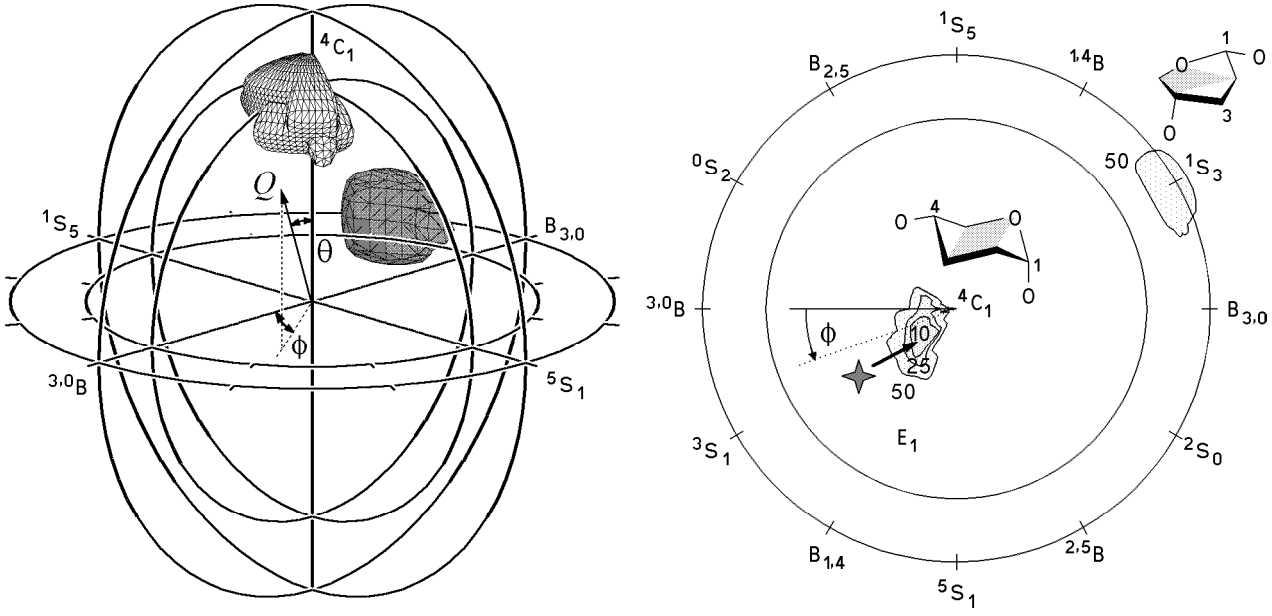

cyclo[D-Glc*p* α(1→4)]$_6$ (**4**)

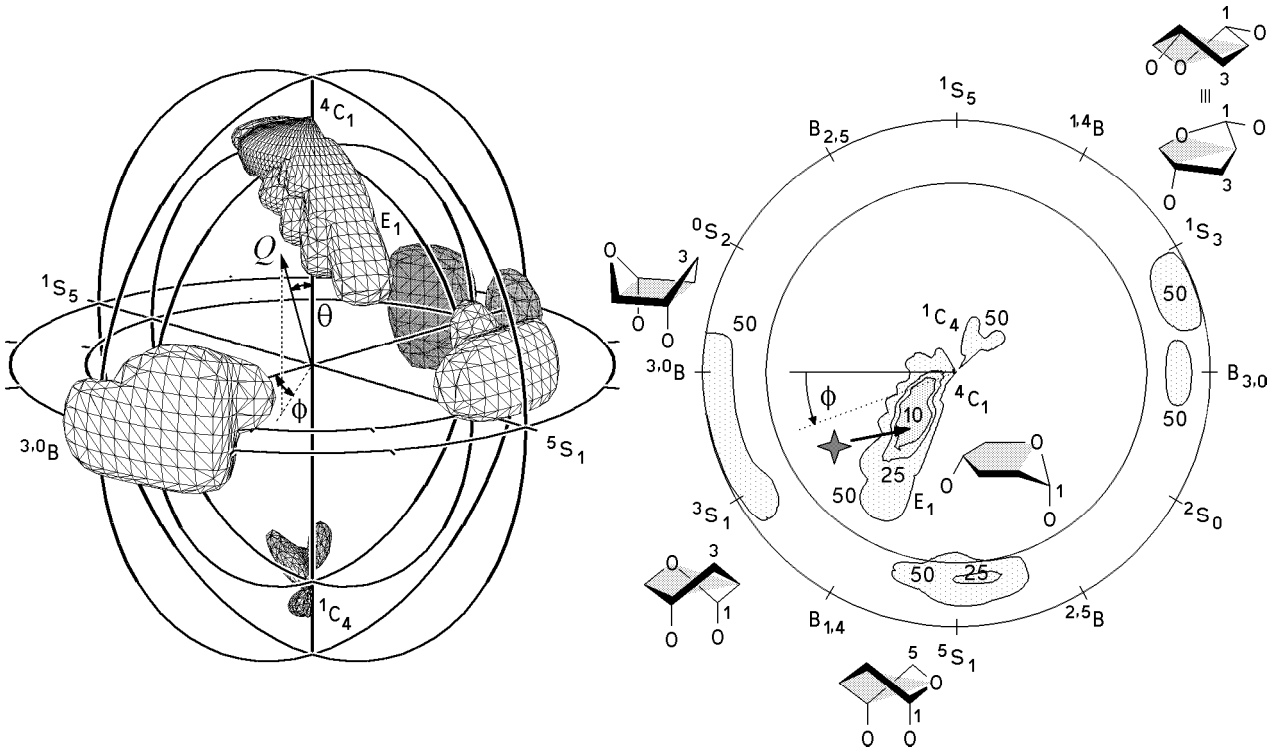

cyclo[D-Glc*p* α(1→4)]$_5$ (**3**)

Fig. 8-4. Iso-energy contour surfaces of total molecular energies (HTA) as a function of the glucopyranose Cremer-Pople puckering parameters Q, θ, and ϕ for α-cyclodextrin (**4**) and its next lower homolog cyclo-α(1→4)-glucopentaoside (**3**). Left diagrams: polar-coordinate plots with a contour value of +50 kJ/mol with respect to the global minimum. The solid circles in the 3D-plots mark constant puckering amplitudes of Q = 0.60 and 0.80 Å. On the *right* side each, projections of the 3D-energy contours into the equator plane (θ = 90°) are shown at relative +10, +25, and +50 kJ/mol levels (the global energy minimum is marked by an asterisk; circles correspond to puckerings of Q = 0.60 and 0.80 Å in the equator plane for θ = 90°). In addition, the relevant glucopyranose conformations are inserted as pictograms.

For the cycloglucopentaoside **3**, the global energy minimum for the pyranose conformations (Fig. 8-4) is still located close to the north pole ($^4C_1$), albeit the energy contours become significantly smoother and more extended than in **4**, and are slightly shifted to larger latitudes (increasing θ) in the direction towards E_1 geometries ($\phi \approx 45°$, cf. Table 8-1). Additional local energy minima of $\approx +25$ kJ/mol in the $^5S_1$-region, and $\approx +50$ kJ/mol for $^{3,O}B \leftrightarrow {}^3S_1$, $B_{3,O} \leftrightarrow {}^1S_3$, and inverted $^1C_4$-conformations, indicate that alternate glucopyranose conformations are energetically more readily accessible in the cycloglucopentaoside **3** than in α-CD (**4**). Obviously, the tension inherent in **3** results in a tendency of both the C_1-O_1 and the C_4-O_4-bonds to adopt pseudoaxial orientations that enable alternate pyranose geometries through release of strain from the macrocycle.

Thus, as a results of the CHARMM study the cyclodextrins also appear to be flexible, but to a less pronounced extent as it was concluded from the MM2 or AMBER calculation, though no exact specification of the structure generation procedure was provided, nor was the nature of the minima thoroughly explored in this investigation[332]. Because of strong interresidue hydrogen bonding between the 2-OH and 3'-OH groups, both studies underestimate the mean tilt angles and predict canting of the glucose units with the 6-CH_2OH towards the outside of the CD ring, an effect which has to be considered as a computational artifact emerging from the vacuum conditions applied for the calculation. The opposite trend is relevant in the CD solid state conformations and in solution: in both cases intramolecular hydrogen bonding is strongly disfavored over intermolecular interactions – including CD–water hydrogen bonds – leading to a widening of the CD torus rim at the 2-OH and 3-OH side.

By the way of summation, the conformational properties of the glucopyranose units in **3** and **4** that emerged from the PIMM91 calculations are fully are fully substantiated by the HTA calculatory data, particularly with respect to the distinct progressive flattening of the pyranose units at C-4 on reducing the ring size. However, the PIMM91 structures (cf. Fig. 8-1) exhibit molecular parameters closest to the corresponding experimental expectation values, most notably, the glucose tiltings are properly reproduced. In addition, these symmetrical geometries represent the best molecular pictures for the time-averaged overall shapes of the cyclodextrins **1** – **4**, and thus, are used in the sequel to further evaluate the physico-chemical properties of small ring cyclodextrins by molecular modeling.

Small Ring Cyclodextrin Contact Surfaces and Cavity Dimensions

Already the cyclodextrin O_1-$O_{1'}$-distances listed in Table 8-1 sustain the notion that of the small ring cyclodextrins only the pentamer **3** is to exhibit a center cavity large

enough to include small guest molecules. To further assess this, the contact surfaces[46], which are closely related to the solvent-accessible surfaces[47], were generated by the MOLCAD-program[48] and depicted in dotted form (Fig. 8-1). For better visualization of the extension of these surfaces and the cavity proportions, cross cuts through the contact surfaces were calculated (cf. Fig. 6-7), and the respective contour lines originating from successive 10° rotation around the geometrical center *M* were superimposed (Fig. 8-5). The effective molecular dimensions displayed by these surface cuts are listed in Table 8-3 and compared to those of the higher cyclodextrin homologs β-CD (**5**) and γ-CD (**6**), for definition of the cavity dimensions see Fig. 8-6.

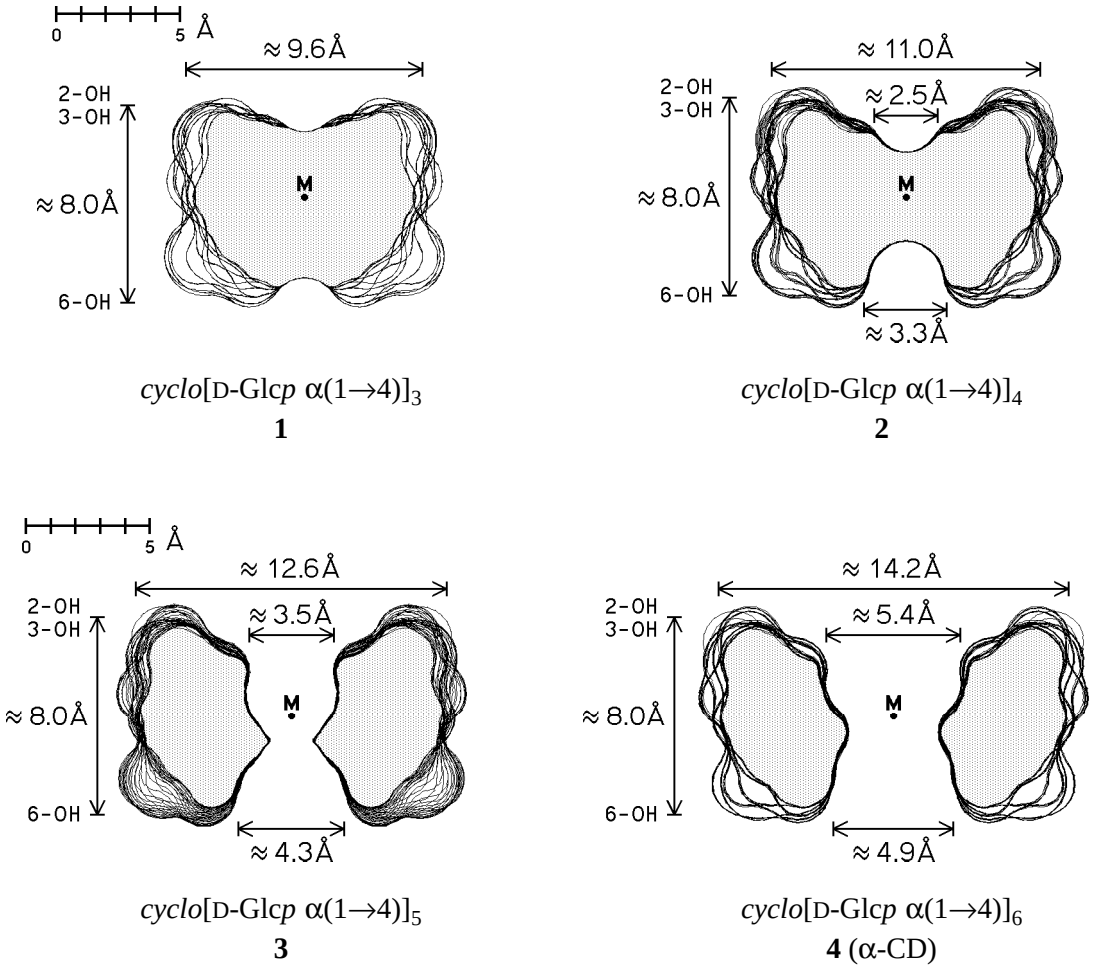

cyclo[D-Glc*p* α(1→4)]$_3$ **1**

cyclo[D-Glc*p* α(1→4)]$_4$ **2**

cyclo[D-Glc*p* α(1→4)]$_5$ **3**

cyclo[D-Glc*p* α(1→4)]$_6$ **4** (α-CD)

Fig. 8-5. Cross section plots of a plane perpendicular to the macrocycle mean plane with the contact surfaces of the cyclodextrins **1** – **4** (cf. Fig. 6-7). Contours were obtained for successive 10° rotation steps around the geometrical center *M* and superimposed. In each case, the wide opened torus rim of the secondary 2-OH / 3-OH groups is on top, and the narrow aperture made up by the primary 6-OH groups on the bottom side; approximate molecular dimensions are included.

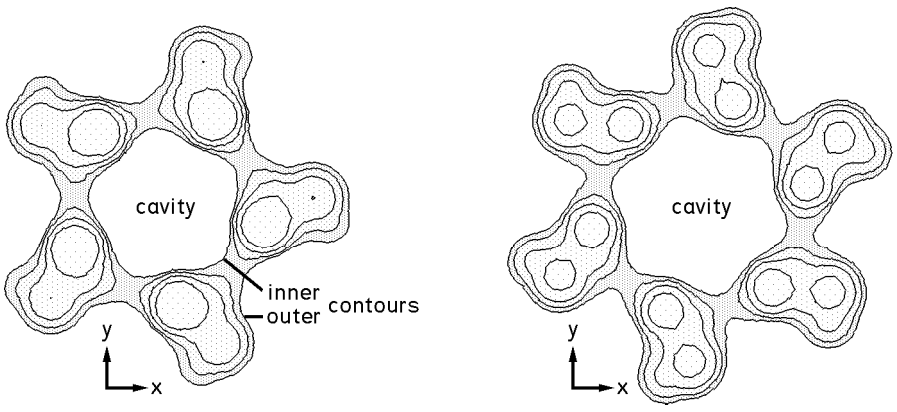

cyclo[D-Glc*p* α(1→4)]$_5$ **3**

cyclo[D-Glc*p* α(1→4)]$_6$ **4** (α-CD)

Fig. 8-6. Mathematical definition of cavity dimensions and volumes: cross section cuts of the cyclodextrins **3** and **4** (α-CD) with planes parallel to the mean plane of the macrocycle (*x* / *y*-planes) were calculated in steps of $\Delta z = 0.05$ Å starting from the top (here the 6-CH_2OH side, i.e. the narrower opening). The topmost and bottommost contours exhibiting separate inner and outer closed cyclic contours were taken as cavity limiting upper and lower boundaries. For clarity, only the four topmost slices, 0.1 Å apart from each other, are shown here.

Table 8-3. Molecular dimensions and cavity characteristics of cyclodextrins **1** – **6** (PIMM91 structures).

cyclodextrin		torus ∅ [Å] outer	inner	torus height	surface area [Å^2] total	cavity	molecular volume [Å^3] total	cavity	exp.[a]
6	γ-CD	17.3	8.4	8.0	960	140	1305	250	1330
5	β-CD	15.7	6.6	8.0	845	105	1140	160	1168
4	α-CD	14.2	5.2	8.0	720	85	975	100	1010
3		12.6	3.9	8.0	605	60	815	50	–
2		11.0	(3.0)[b]	8.0	475	(15)[b]	660	(5)[b]	–
1		9.6	–	8.0	370	–	495	–	–

a) Apparent molar volume $^{\phi}V$ for dilute aqueous solutions[356]. – (b) Surface dent only, no cavity.

In essence, the well-established conical doughnut shape of the native cyclodextrins **4** – **6** is retained in the smaller analogs **1** – **3**, with the wide-opened rim of the torus being made up by the 2-OH and 3-OH groups, the narrower aperture carrying the 6-CH_2OH groups. The respective tori exhibit essentially constant heights of approximately 8 Å (cf. Fig. 8-5). As is also clearly evident, the pentameric cyclodextrin **3** features a central cavity similar, yet distinctly smaller than the α-CD (**4**), the inner

diameter being less than 4 Å. In the tetrameric homolog **2**, and in the trimer **1**, there is no cavity at all, instead **2** exhibits a substantial indentation on the top and bottom sides of the cone (Fig. 8-5), whereas **1** features only a shallow surface dent, and thus resembles more closely a solid frustum rather than a torus.

The cavity interior comprises approximately 10 – 15% of the total cyclodextrin surface area (Table 8-3, ≈ 120 Å^2 / glucose unit). The spatial volume included by the contact surfaces closely corresponds to the apparent molar volume $^{\phi}V$ required by these compounds in aqueous solution. The conformity of the values calculated for the native cyclodextrins **4** – **6** (Table 8-3, ≈ 160 – 165 Å^3 / glucose unit) with the volumes obtained from density measurements in aqueous solution[356] indicates the central hole to be occupied by water molecules, otherwise much larger apparent volumes would have to be observed. In the case of α-CD hexahydrate, crystal structural data[337-339] revealed an asymmetrically distorted cavity of approx. 5 Å width and a volume of ≈ 100 Å^3, able to accommodate two water molecules ($^{\phi}V_{H2O}$ ≈ 30 Å^3) in well-defined positions. The high pressure inclusion of krypton – with its van der Waals diameter of ≈ 4.0 Å krypton is comparable in size to a water molecule – leads to less distorted α-cyclodextrin solid state structures, in which krypton only fits loosely the cavity with a statistical positional distribution[373]. The comparison of both the water and krypton inclusion complexes of α-cyclodextrin, clearly indicates the flexibility of the cavity for adopting towards different guest molecules[373].

From the cavity volume of approx. 50 Å^3 calculated for the cyclopentaoside **3**, it may be inferred that it should exhibit complexing capabilities for at least small molecules, provided that the pocket also exhibits a certain degree of flexibility. The noble gases krypton (van der Waals radius ≈ 1.9 Å), argon (r_{VDW} ≈ 1.8 Å), and neon (r_{VDW} ≈ 1.5 Å) might fit into the cavity, as well as one molecule of water. The latter hypothesis should be the most easiest to be verified: comparison of the experimental apparent molar volume determined by simple density measurements of aqueous solutions of **3** and comparison with the calculated volume of ≈ 815 Å^3 (Table 8-3) may result in a direct proof for inclusion of water.

Molecular Lipophilicity Pattern (MLP) of Small Ring Cyclodextrins

Aside from the imperative fulfillment of steric requirements, the hydrophobic effect[116,117] represents the most important factor in governing guest-host interactions in the cyclodextrin series[305-308]. Concomitantly, the release of complexed water out of the cyclodextrin cave and the hydrophobic hydration sphere[117] of the guest to be incorporated into the bulk water phase must be considered as the main entropic factor favoring complex formation. The color-coded visualization of **m**olecular **l**ipophilicity

patterns (**MLP**'s)[58] projected onto molecular contact surfaces by using the MOLCAD-molecular modeling program[48,59] is especially suited for the assessment of hydrophobic interactions. The MLP's for the four cyclooligosaccharides **1** – **4** are depicted in Figs. 8-7 and 8-8 in a two color code graded into 32 shades, ranging from dark-blue for the most hydrophilic areas to yellow-brown for the most hydrophobic regions (cf. footnote on p. 75).

The MLP's of the cyclodextrins reveal the 2-OH / 3-OH side of the macrocycles, i.e. the respective wider torus rim, to be distinctly hydrophilic (Fig. 8-7, top entry, with clearly defined blue areas). This is contrasted by the intensely hydrophobic (yellow-brown) surface regions on the opposite side – the narrower opening made up by the 6-CH_2OH groups – which in the case of α-CD (**4**) and the pentamer **3** extend well into the cavity. For the smaller cyclodextrins **1** and **2**, devoid of a cavity penetrating the macrocycle, the respective center indentation (**2**) and the shallow surface dent (**1**) are the most hydrophobic regions. An even more articulate impression of the MLP's is provided by the juxtaposition of the respective side-views in closed and half-opened form (Fig. 8-8).

Accordingly, the cycloglucopentaoside **3** is surmised not only to be capable of inclusion of small molecules on geometrical grounds, but also on the basis of its hydrophobicity characteristics, which closely resemble those of α-CD (**4**). Only the narrower cavity substantially limits the type of molecules to form inclusion complexes – noble gases being adequate candidates in terms of geometry and hydrophobic interactions. The two smaller cyclodextrins **1** and **2** – if ever synthesized – should exhibit binding of hydrophobic molecules in a sandwich type manner only.

Fig. 8-7. (opposite page). MOLCAD-program generated molecular lipophilicity patterns (MLP's) projected onto the contact surfaces of *cyclo*[Glcα(1→4)]$_3$ (**1**, *upper left*), *cyclo*[Glcα(1→4)]$_4$ (**2**, *upper right*), *cyclo*[Glcα(1→4)]$_5$ (**3**, *lower left*), and *cyclo*[Glcα(1→4)]$_6$ (**4**, α-CD, *lower right*). Color-coding was carried out cf. footnote on p. 75, blue shading represents most hydrophilic surface areas and yellow-brown colors indicate most hydrophobic regions. The *top* picture views through the larger openings of the conically shaped molecules, exposing the intensively hydrophilic (blue) 2-OH / 3-OH side. In the *middle*, the hydrophilic front half of the surface has been removed providing an inside-view onto the hydrophobic (yellow-brown) backside. In addition, a ball and stick model was inserted to illustrate the molecular orientation (mode of viewing analog to Fig. 8-1). The *bottom* representation depicts the "backside" (i.e. the smaller opening with the 6-CH_2OH groups facing the viewer) of the cyclodextrins, clearly exposing the hydrophobic (yellow-brown) surface areas that in the case of **3** and **4** extend well into the cavity.

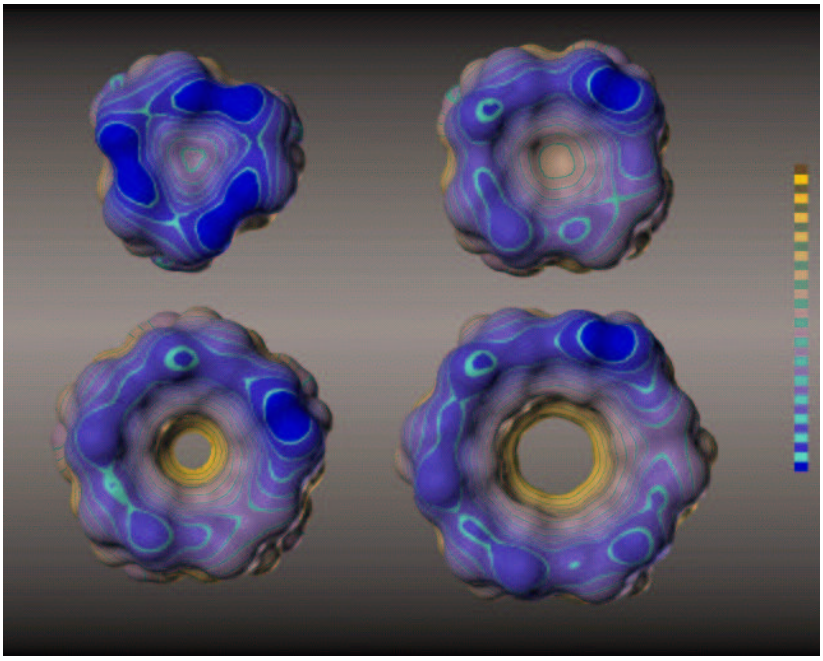

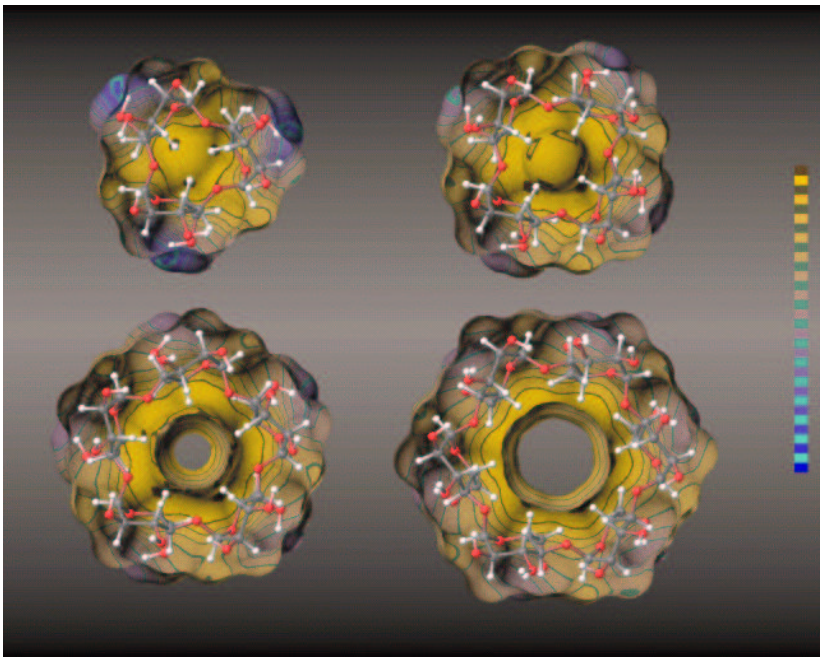

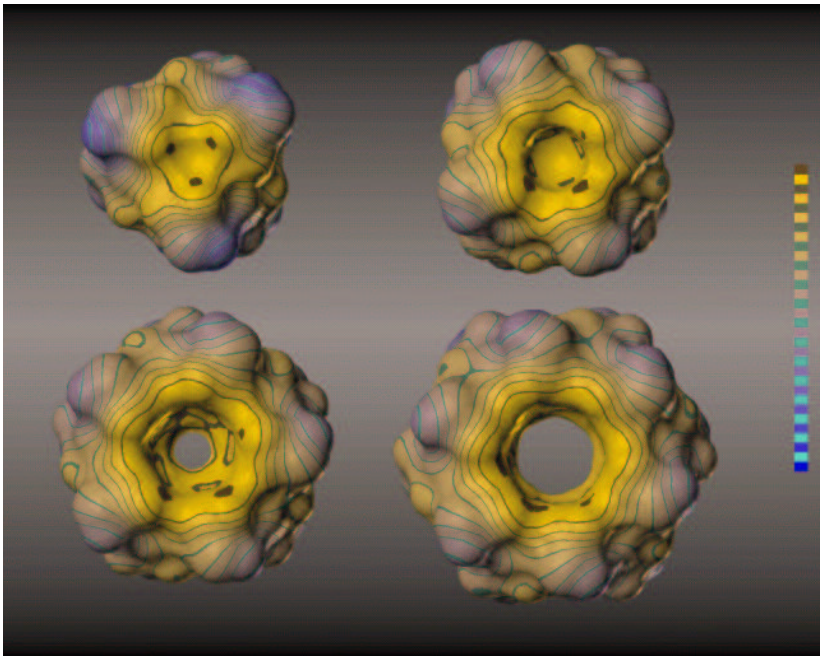

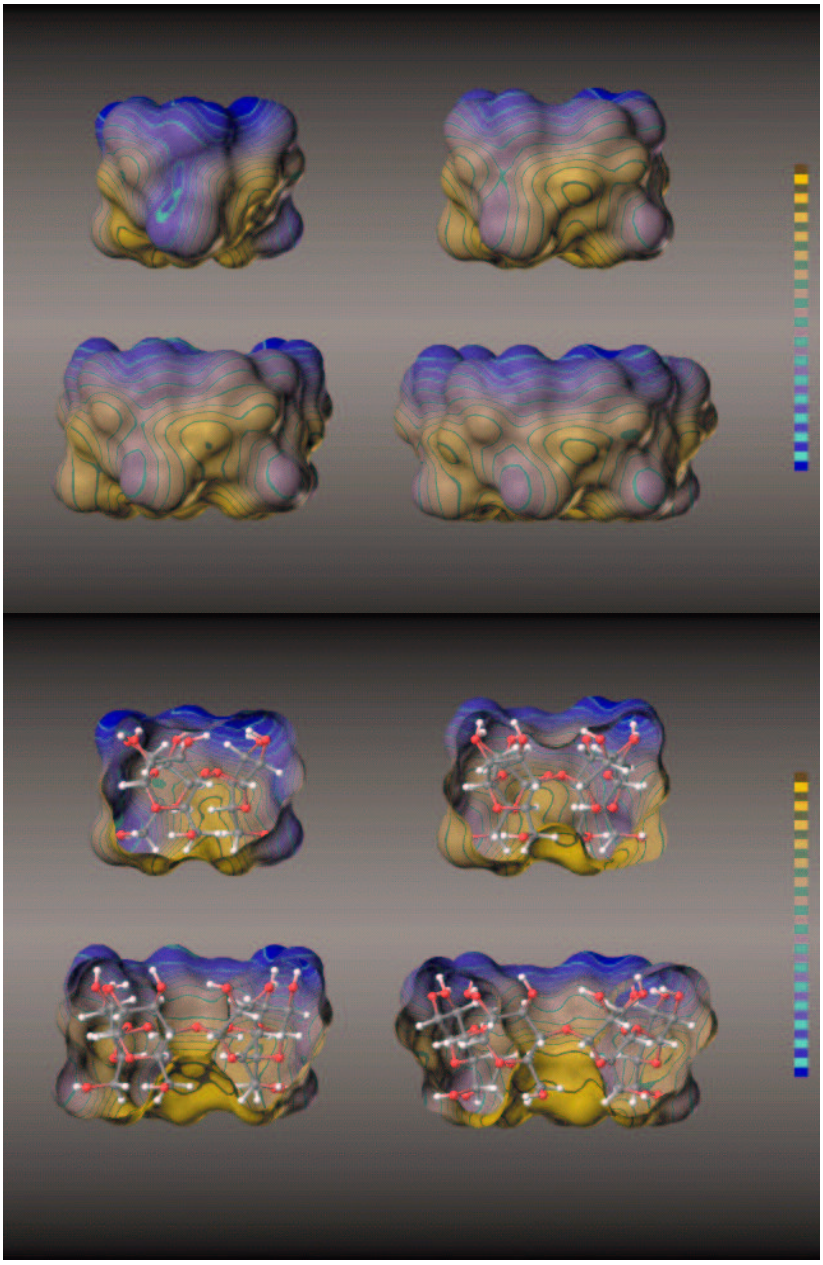

Fig. 8-8. Side view MLP's, in closed and bisected form each, of the four α(1→4)-cyclodextrins **1** – **4** with three (**1**, *upper left*), four (**2**, *upper right*), five (**3**, *lower left*), and six (**4**, α-CD, *lower right*) glucose units, respectively; color-coding according to Fig. 8-7. Their orientation is uniformly such that the 2-OH / 3-OH side (larger opening of the torus) is aligned upward and the 6-CH_2OH (smaller aperture) points downward. The similarities in the distribution of hydrophilic (blue) and hydrophobic surface areas – most notably on the inside regions of the cavities of **3** and **4** (*lower rows*, each) – are clearly apparent.

Conclusions

The molecular modelings presented clearly provide a concise picture of cyclodextrin features – in terms of their geometrical and conformational properties as well as their molecular lipophilicity patterns (MLP's) – as a function of their ring

size. Some properties well established for α-CD (**4**) are uniformly maintained throughout the entire series of small ring cyclodextrins **1** – **3**, i.e. the tilting of the glucose units in respect to the macrocycle, for example, whilst others, most notably the puckering of the pyranose units, change substantially in the smaller homologs. On the basis of the calculatory data, the proposition of large steric strains to be responsible for the absence of at least the "unnatural" cyclopentaoside **3** in the enzymatic digestions of starch has to be discarded. However, the increasing strain energy in **2** and finally **1**, has far-reaching implications on the chances of these compounds ever to be synthesized being rather dim, but not entirely illusive.

Contraction of the cyclodextrins by successive excision of one glucose unit from the ring expresses itself most significantly in a clear narrowing of the central cavity, the cycloglucotetraoside **2** and the trioside **1** even lacking a hole penetrating the macrocycle. The hydrophobicity pattern of the pentamer **3** resembles closely to that of the native α-CD (**4**), and by consequence must lead to the conclusion that the largest of the small ring cyclodextrins should be capable of forming inclusion complexes with small molecules of appropriate dimensions. In contrast to this, the homologs **2** and **1** should be amenable for hydrophobic binding via their surface indentation only, the formation of inclusion complexes is expected to be impossible.

Appendix – Computational Methods

I. Glucose Tilt Angle τ Variations: For generation of the structures of the native α-CD (**4**) and its small-ring analogs **1** – **3**, PIMM91-geometry optimized glucose $^4C_1$-conformations exhibiting different hydroxymethyl torsions[66] (*gg*, ω = -60°, and *gt*, ω = +60°) were assembled to form symmetrical structures (i.e. all O_1 / $O_{4'}$-atoms forming a regular *n*-polygon) by using a rigid body rotation and fitting procedure[128]. Thereby, the glucose tilt angles τ were varied in the range of +60 – +140° in steps of 5°. After geometrical repositioning of all CH- and OH-hydrogen atoms, avoiding close steric contacts and considering different hydroxyl group torsions, each structure was fully optimized without any restraints by using the PIMM91 force field program[45] for *in vacuo* conditions (ε = 1). The resulting global minimum energy structures given in Fig. 8-1 were used for the generation of the contact surfaces and molecular lipophilicity patterns (MLP's).

II. HTA Calculations: For determination of the lowest molecular energy conformations of the pentamer **3** and the hexameric α-CD (**4**) by high temperature annealing (HTA)[456], a modified force field specially adapted for carbohydrates[454] was used. The Verlet integrator[458] was applied in the MD simulation program CHARMM[459] with a timestep of 1 fs at constant temperature[460] and a dielectric

constant $\varepsilon = 1$. Out of MD trajectories at 1200 K (4382 ps for **3**, 2000 ps for **4**) every 1000 fs the respective conformation was allowed to cool down to 300 K with a rate of 10 K/fs, was held there for additional 1010 fs, and was subsequently fully energy-minimized by an adapted Newton-Raphson algorithm of the CHARMM22 program package[459] with a convergence criterion of 10^{-7} kcal/mol.

In the case of the cycloglucopentaoside **3**, a total of 3264 (75%) different conformers (corresponding to 16320 glucose units) were entered into geometry analysis, in the case of α-CD (**4**) a total of 1675 (84%) structures (10050 glucose residues) were used. All molecular parameters and root-mean-square (RMS) deviations were determined by Boltzmann-weighted averaging (300 K) using the total cyclodextrin energies.

III. Energy Potential Surfaces and Contour Plots: For computation of the cyclodextrin energy potential surface as a function the Cremer-Pople parameters[122,124], the HTA data set $\Delta H_F^{298} = f(Q, \theta, \phi)$ of **3** and **4** was divided into classes $[Q + \Delta Q, \theta + \Delta\theta, \phi + \Delta\phi]$ for the 3D-plot (Fig. 8-4, $\Delta H_{rel} \approx 0 - 230$ kJ/mol, $0.52\,Å \le Q \le 0.84\,Å$, $0° \le \theta \le 180°$, and $0° \le \phi \le 360°$, width of classes $\Delta Q = 0.05$ Å and $\Delta\theta = \Delta\phi = 10°$) and classes $[Q \sin\theta, \phi]$ for 2D-contouring (window size $\Delta(Q \sin\theta) = 0.05$ Å and $\Delta\phi = 10°$). For each class, energies were Boltzmann-averaged (300 K). The contour plots were computed using cubic regression formulas and were plotted in polar coordinates[163].

IV. Molecular Surfaces and Lipophilicity Profiles: Calculation of the molecular contact surfaces and molecular lipophilicity patterns was carried out using the MOLCAD[48] molecular modeling program and texture mapping[59], a detailed description of the computational basics is given in Chapter 3. Scaling of the hydrophobicity profiles was performed in arbitrary units and in relative terms for each molecule separately, no absolute values are displayed (no significant differences are observed applying absolute overall scaling). Color graphics were photographed from the computer screen of a SILICON-GRAPHICS workstation.

Acknowledgement: I am grateful to Prof. Dr. J. BRICKMANN and Dr. S. REILING, Technische Hochschule Darmstadt, for providing the MOLCAD molecular modeling software package for computer graphics, and for assistance performing the HTA analysis of **3** and **4** with their modified CHARMM force field.